Three-dimensional preparation and imaging reveal intrinsic microtubule properties

Philipp J Keller, Francesco Pampaloni & Ernst H K Stelzer

Supplementary figures and text

Supplementary Figure 1: Sample preparation of egg extracts in custom Teflon-based cylinders.

Supplementary Figure 2: Tracking time series for a MT.

Supplementary Figure 3: Illustration of the processing steps of the automated 3D MT contour detection subroutines provided by the program "processTL".

Supplementary Figure 4: Flow-chart of 3D image processing and 3D data analysis routines.

Supplementary Table 1: Comparison of parameters describing 2D and 3D MT dynamic instability in interphasic *Xenopus laevis* egg extracts.

Supplementary Methods

Note: Supplementary Software and Supplementary Videos 1–4 are available on the Nature Methods website.

Supplementary Figure 1: Sample preparation of egg extracts in custom Teflon-based cylinders

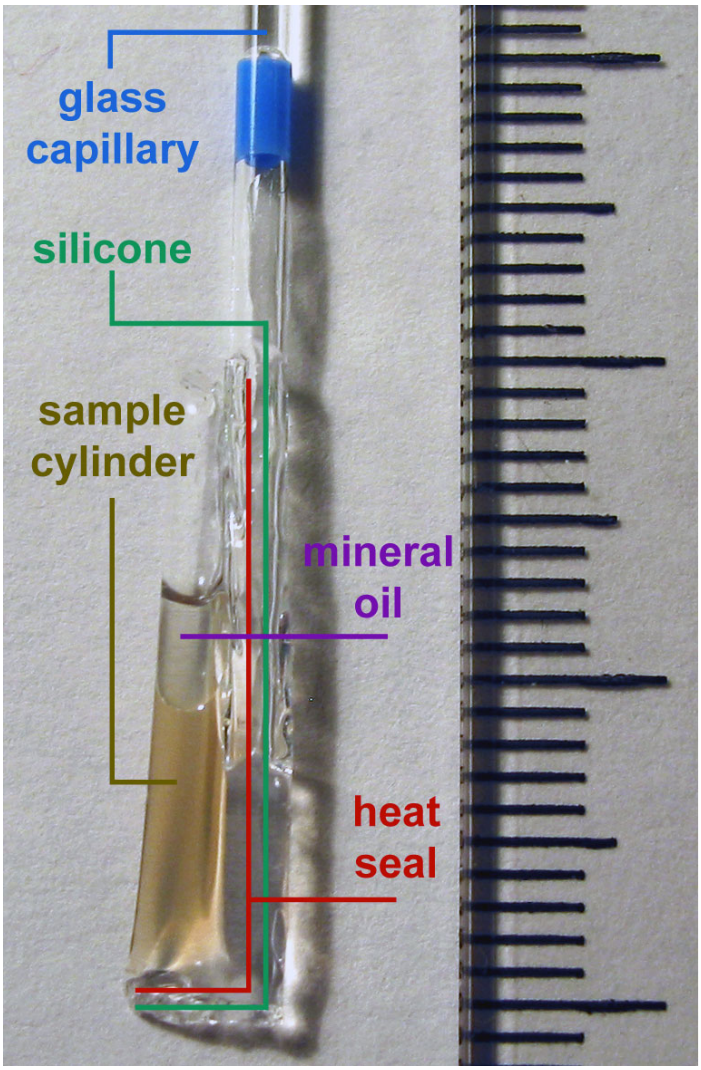

The photo shows a polytetrafluorethylen (PTFE) cylinder loaded with egg extract as employed in the 3D experiments. The cylinder is formed using a 25 µm thin PTFE foil. By application of heat, the bottom part and the seam of the cylinder are sealed. A glass capillary is glued to the cylinder with silicone. The heat seal prevents contact of the silicone with the inside of the PTFE cylinder. For the loading of the extract, the cylinder is put on ice. 20 µl egg extract (at 4°C) are pipetted into the cooled-down cylinder. A layer of mineral oil is added to prevent extract degradation by exposure to oxygen in the air. Finally, the cylinder is mounted in the SPIM imaging chamber, where it is surrounded by distilled water at 20 °C. Temperature measurements showed that the sample cylinder equilibrates to 20 °C within 20 s.

Supplementary Figure 2: Tracking time series for a MT

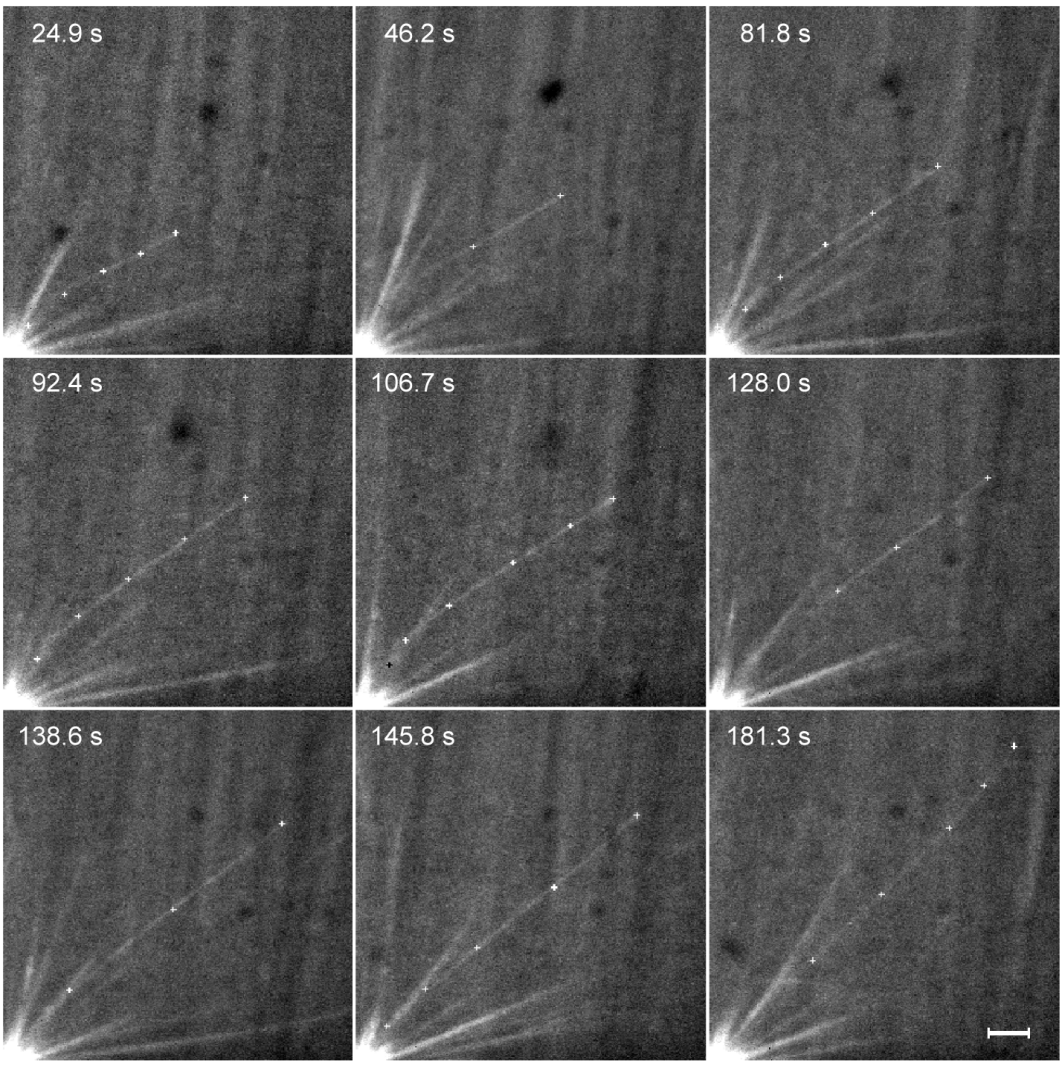

The SPIM slice that contains the MT's tip is shown for nine time points of a MT dynamics data set. The white crosses represent the manually defined trace of the respective part of the MT that is visible in the corresponding z-slice. In frames 2 and 6, a considerable part of the MT's 3D geometry is located in slices other than that containing the MT's tip. The visualization LUT has been reduced to 9 bit (from originally 12 bit in the raw data). While this reduction helps in manual MT tracking, it artificially expands the centrosome region. Thus, a visualization LUT with a larger dynamic range is typically chosen for the tracking of very short MTs. The white bar represents 5 µm.

Supplementary Figure 3: Illustration of the processing steps of the automated 3D MT contour detection subroutines provided by the program “processTL”

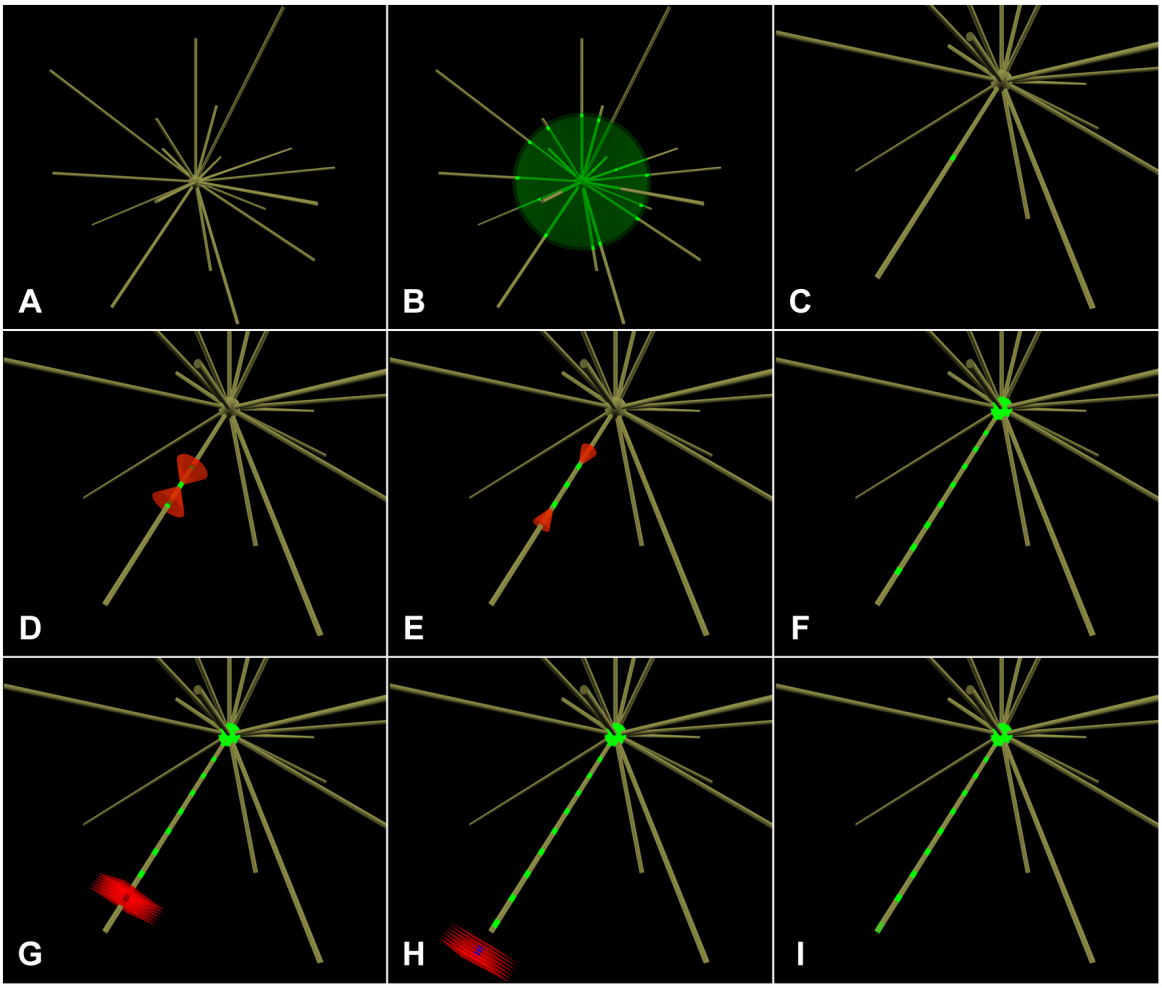

Detailed explanations are provided in the section “Automated 3D MT contour detection”.
(**a**) A schematic digital MT aster. (**b**) Mapping of a spherical surface around the centrosome with highlighted MT intersection points. (**c**) Tracing start point (obtained in **b**) for one single MT. (**d**) Initial bidirectional conical tracing along the filament. (**e**) Accumulation of contour points along the filament. (**f**) Detection of the MT minus-end in the proximity of the centrosome. (**g**) Analysis of the fluorescence standard deviation in planes perpendicular to the tracing direction for MT plus-end detection. (**h**) Tracing overshoot triggers plus-end tracing with a smaller step size (pixel-by-pixel analysis). (**i**) The algorithm stops, when the entire MT contour from minus-end to plus-end is characterized.

Supplementary Figure 4: Flow-chart of 3D image processing and 3D data analysis routines

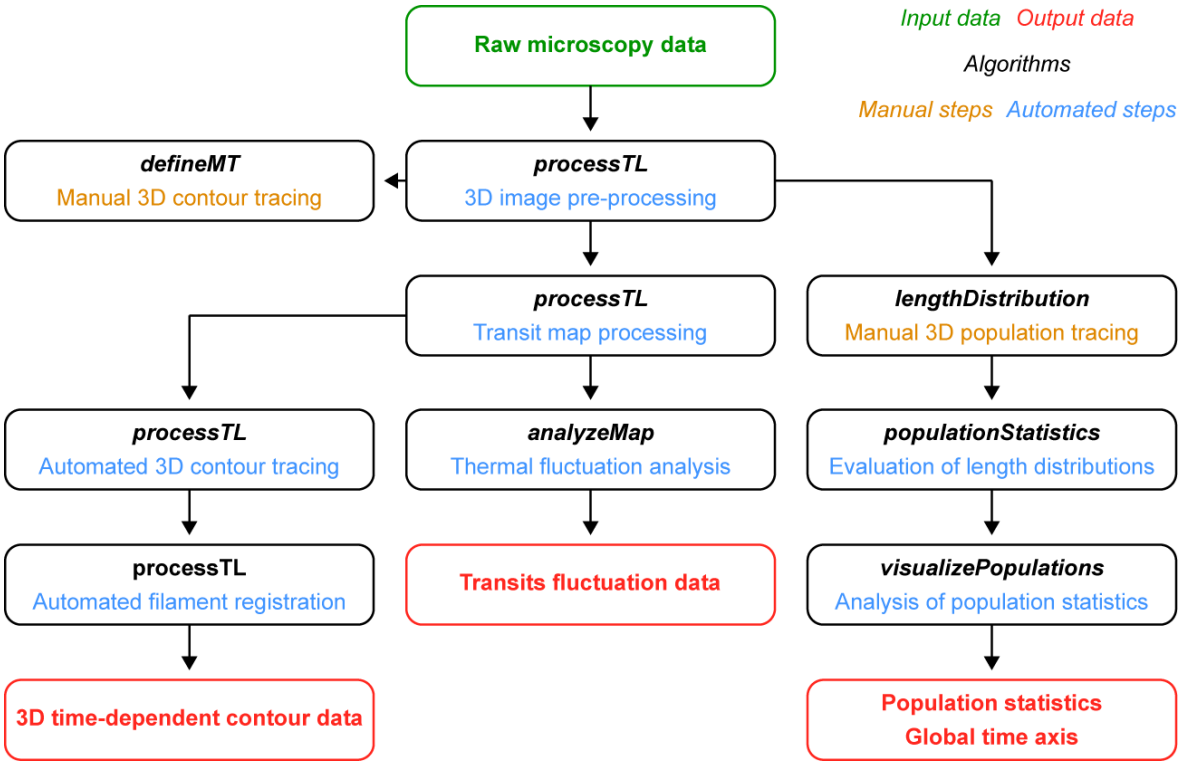

MT 3D contour tracing can be performed both automatically (with “processTL”) or manually (with “defineMT”). This study’s results on 3D MTDI were obtained by manual tracing with “defineMT”. An approach to a fully automated image processing is explained in the section “Automated 3D MT contour detection” (see also **Supplementary Video 4** and **Supplementary Figure 3**).

Supplementary Table 1: Comparison of parameters describing 2D and 3D MT dynamic instability in interphase *Xenopus laevis* egg extracts

reference & system	average v_g [µm min^{-1}]	SD of v_g [µm min^{-1}]	average v_s [µm min^{-1}]	SD of v_s [µm min^{-1}]	J [µm min^{-1}]	p_{growth}	$p_{shrinakge}$	p_{pause}
[6] 2D	22.7	7.9	15.2	9.5	–	0.655	**0.163**	0.182
this study 2D	18.9 ± 0.3 (*n* = 172)	4.5 / 7.0‡ (*n* = 172)	12.1 ± 0.8 (*n* = 70)	6.9 / 8.8‡ (*n* = 70)	–	0.660	**0.269**	0.071
this study 3D	10.9 ± 0.6 (*n* = 140)	6.5 / 8.1‡ (*n* = 140)	12.8 ± 1.9 (*n* = 20)	8.3 / 9.2‡ (*n* = 20)	9.1 ± 1.2 (*n* = 5)*	0.772	**0.021**	0.207

The data in Niethammer *et al*. 2007 (reference 6 in the main text) were derived under comparable experimental conditions with respect to the egg extract system and the time points of data acquisition and are consistent with the 2D data obtained in this study. All indicated errors are errors of average values, except for the parameter *J*, for which the standard deviation is shown.

* The population statistical parameter is an average of five experiments. Approximately 300 independent MT length measurements were performed in each of these experiments (see **Figure 4**).

‡ The first value represents the observation-time-weighted standard deviation. Since the correction with phase observation times was not performed in Niethammer *et al*., the corresponding uncorrected standard deviation is also provided (second value). The second value should therefore be used for a comparison of the 2D results.

SUPPLEMENTARY METHODS

Preparation of fresh interphase *Xenopus laevis* egg extracts

The experimental results are based on in total 18 independent experiments that were performed with 12 different freshly prepared interphase egg extracts.

Undiluted cytoplasmic egg extracts were prepared from *Xenopus laevis* eggs as previously described by Murray[1], with some modifications. After dejellying and washing, the eggs were transferred to centrifuge tubes containing CSF-XB plus protease inhibitors and 10 µg/ml cytochalasin D (Sigma-Aldrich, St. Louis, MO, USA). The packing spin was performed for 30 seconds at 500 rpm, then for 90 seconds at 2.000 rpm and room temperature with a Heraeus Megafuge 1.0R. The centrifuge tubes were then transferred to a Beckman Coulter JS-13.1 rotor at room temperature. The crushing spin was performed for 20 minutes at 11.000 rpm and 4 °C. After collecting the cytoplasmic fraction 10 µg/ml cytochalasin D were added. The meiotically CSF-arrested extracts were then split into 100 µl aliquots and treated with 0.4 mM $CaCl_2$ and 0.7 mM cycloheximide (Sigma-Aldrich, St. Louis, MO, USA) and incubated for 90 min at 20°C to obtain interphase extracts.

Three-dimensional sample preparation

For each experiment, 25 µl of fresh interphase egg extract were gently mixed with 1.5 µl undiluted centrosomes and 1 µl Alexa-488 labelled tubulin (74 ± 1 µM, 38 ± 2 % labelling ratio) at 4°C. Thus, assuming an average contribution of 18 µM tubulin from the egg extract[2] 5 % of the tubulin were fluorescently labelled. In order to obtain a good contrast in the 2D experiments, 0.3 µl Cy3-labelled tubulin (101 µM, 178 % labelling ratio) were added instead of Alexa-488 labelled tubulin. A regenerative oxygen-scavenging system was prepared by mixing 10 µl catalase (10 mg/ml, Sigma-Aldrich, St. Louis, MO, USA), 10 µl glucose oxidase (10 mg/ml, Sigma-Aldrich), 10 µl glucose (1 M) and 3 µl Haemoglobin (Sigma-Aldrich, St. Louis, MO,

USA) saturated buffer at 4°C. 1 µl of the system were added to the egg extract. 20 µl of this mix were then transferred to a Teflon-based cylinder (see reference 14 in the main text) at 4°C. 5 µl mineral oil were layered on top of the sample in the cylinder. Before mounting the cylinder in the SPIM, the mix was equilibrated in the cylinder at 4°C for three minutes. The SPIM imaging chamber was equilibrated to 20°C 1 hour prior to mounting of the cylinder. Over the entire course of the experiment the imaging chamber's temperature was kept constant at 20°C.

Three-dimensional imaging

Our observation system for 3D imaging of MT dynamics is based on one of EMBL's implementations of light-sheet based fluorescence microscopy (Single Plane Illumination Microscopy or SPIM, see reference 13 in the main text). Alexa-488 molecules were excited with a Melles Griot argon gas laser at 488 nm. Fluorescence was detected via a Carl Zeiss Achroplan W 100x/1.0 water dipping objective and a Semrock RazorEdge long pass filter (> 488 nm). Data were recorded with a Hamamatsu Orca camera at 2x binning with a temporal resolution of 3.6 sec per image stack (29 frames) and a spatial resolution of 300 nm laterally and 1500 nm axially for an imaging volume of 87 x 66 x 20 µm³. The voxel size in the data sets is 129 x 129 x 700 nm^3. Data analysis was performed directly on the raw data sets (see below).

In order to generate the light sheet, the laser's Gaussian beam profile is first reshaped by a set of apertures. The resulting profile is subsequently focused along one dimension by a cylindrical lens (01 LQC 006, Melles Griot, Rochester, NY). For high-magnification experiments, an additional objective (Epiplan 10x/0.2, Carl Zeiss, Jena) is introduced to the microscope's illumination system[3]. Since the illumination objective swaps the focused dimension with the unfocused dimension, the cylindrical lens has to be tilted by 90 degrees around the optical axis as compared to the orientation in the first implementation of the microscope. The combination of a cylindrical lens with an illumination objective provides both a sheet-shaped illumination profile (due to the cylindrical lens) and a sufficiently high numerical aperture (due to the illumination objective) to focus the light sheet down to a thickness of 1500 nm.

Two-dimensional imaging

2D imaging was performed on a Carl Zeiss Axiovert 135 TV. Time-lapse data sets were recorded with MetaMorph (version 6.3r2) with a temporal spacing of 2 s. For each image, the sample was illuminated at 543 nm for 200 ms at 80% of the maximum output power of an HBO 100 high-pressure lamp. Fluorescence was detected using a Carl Zeiss Plan-Apochromat 100x/1.4 oil immersion lens and a Photometrics CoolSnap HQ camera at 2x binning and 10 MHz digitizing rate.

Three-dimensional data analysis of MT dynamics

For the purpose of analyzing 3D data sets of MT dynamics over time, custom processing routines were developed in Matlab (The MathWorks, Natick, MA, USA). The software package facilitates the image processing of 2D and 3D time-lapse data of dynamic MT asters. It consists of algorithms for image pre-processing, manual and automated MT tracing and for the analysis of MT population statistics. Since the algorithms are only sparsely annotated, a brief description of all programs shall be provided here (see also the task flow diagram in **Supplementary Figure 4**). The source code is available on the Nature Methods website.

Image processing programs (including graphical user interfaces):

(1) **processTL**

This tool provides routines for image pre-processing (ROI definition, axial interpolation, detection of the centrosome). The program generates 3D image stacks from the raw microscopy data that are re-centred with respect to the centrosome and cropped according to the user's settings. The position of the MT aster's centrosome is calculated by determining the intensity's centre-of-mass after applying a threshold at 95 % (for 3D SPIM data sets with a high dynamic range) or 60 % (for conventional 2D data sets with a low dynamic range) of the intensity interval defined by the image stack's minimal and maximal intensity values. Subsequently, an algorithm compensates

for the aster's translational movement by re-centring the image stacks with respect to the calculated positions of the centrosome. The program provides options for the mapping of MT transits through a sphere around the centrosome (see **Supplemental Figure 3b**), for the automated tracing of MT contours over time and for a temporal MT registration, allowing to identify MTs at different time points. The program includes a graphical user interface. processTL operates directly on the raw microscopy data.

(2) **analyzeMap**

The program operates on the MT transit mapping data, which is provided by processTL and allows to quantify the thermal fluctuations of MT transits through a sphere around the centrosome with a user-specified radius. The program contains routines for the temporal identification of MT transits and an automated rotational drift correction that allows tracking relative transit coordinates independently of the MT aster's rotational and translational movements.

(3) **defineMT**

The program operates on the re-centred image stacks that are provided by processTL and allows for the manual tracing of MTs over time. The user is able to move along the spatial and temporal axis, while viewing slices of the 3D MT aster. The definition of 3D structures is facilitated by clicking at the corresponding coordinates in the images (see **Supplementary Figure 2**). The program has to be located in the "interpolation" directory that is generated by processTL. All geometrical tracing data presented in this paper were obtained with this routine. In our analysis, we provided up to ten tracing points per MT and time point. Long and strongly bent MTs required more tracing points than short and straight MTs.

(4) **lengthDistribution**

Similarly to defineMT, this program displays the re-centred image stacks of the dynamic MT asters. The user interface has been optimized for the manual tracing of entire MT populations that are required for MT population statistical analyses.

Note that programs (2)-(4) require pre-processing data that is generated by the program processTL and will therefore not operate unless these data are available.

Data analysis programs (no GUIs, operate on data from programs (1)-(4)):

(5) **populationStatistics(*p1*, *p2*)**

This routine analyses the data that is obtained with lengthDistributions. The average population growth speed J and the start time point of MT aster growth are computed from these data sets. The program has to be located in the "interpolation" directory that is generated by processTL. Parameter *p1* indicates the temporal spacing in the 2D/3D recordings (in seconds); parameter *p2* corresponds to the pixel size in the processed images (in μm).

(6) **visualizePopulations(*p*)**

The algorithm analyses the population statistical measurements and computes the global average population growth speed as well as the precision of the global time axis. All measurements are visualized in an overview plot (by individually shifting each series on the length axis according to a user-defined shifts vector $\vec{p}$).

The dynamic phases are determined on the basis of the MT length-over-time diagrams. The processing kernel is based on an algorithm introduced by Gildersleeve *et al.*[4]. For each coordinate in the MT length-over-time diagram, a second-order polynomial fit is applied to a range of N data points to either side. The resulting slope of the fit at the respective coordinate was used to classify the MT's state at that time point. A slope with an absolute value smaller than $v = 2\sigma_{length} / \left(2Nt_{\text{interval}}\right)$ was considered as a pause. σ_{length} is the spatial error of the measurements and $t_{interval}$ the time interval between two MT length measurements. Thus, v denotes the maximum speed that can statistically result in a non-dynamic MT's length-over-time diagram due to the spatial error of the measurement. Larger fitting speeds were attributed to growth or shrinkage, depending on the sign. N was chosen as 5, in order to adopt criteria that are consistent with the existing literature[4].

Additionally, an analysis of multiple dynamic phases was performed. Each growth or shrinkage phase that is identified by the algorithm is analyzed by linear regression. In a reference analysis, the χ^2-value of a linear fit to the entire detected dynamic phases is computed. The probability of the linear (i.e. two-parameter, $n = 2$) model to describe the data set is $p_2\left(\chi^2\right) = \exp\left\{-\chi^2/2\right\}$.

In the next step, the dynamic phase's time interval is split into k sub-intervals (each containing at least three data points) and k linear fits are computed to the data points within these k sub-intervals. All possible combinations of sub-divisions of the original phase are considered. Again, the probabilities for the k fits are computed and the resulting p-values are multiplied. If the product of the probabilities is smaller than the reference probability, the reference probability is replaced by the new value and the parameters characterizing the sub-division of the phase are stored. This multi-phase fit analysis is performed for $k = 2$, 3, 4 and 5. The dynamic phase characterization with the best overall p-value is stored. Increasing k_{max} from 3 to 5 resulted merely in a 2 % increase of the standard deviation of the growth speed distribution. Therefore, we consider the computation of speed switching using $k_{max} = 5$ to be sufficiently accurate. It should be noted that computation time increases exponentially with k_{max}.

Automated three-dimensional MT contour detection

The automated processing routine "processTL" includes subroutines for an automated 3D contour detection in a time-lapse data set. The purpose of these routines is the spatial tracing and temporal tracking of MTs, i.e. the geometrical reconstruction of all of an aster's filaments in 3D and their temporal identification over time. The control of robustness that is necessary when tracing 3D structures automatically with "processTL" consumes about as much time as a semi-automated processing with "defineMT". Thus, the results presented in this work are based on MT contour data that were derived using the program "defineMT". However, some of "processTL"'s image processing routines are also employed in our analysis (in particular, the centrosome detection and correction for translational movements) and hence, the fully automated tracing routines shall be briefly described.

The routines work directly on the raw microscopy data. No intermediate preprocessing is necessary, apart from the image cropping and interpolation steps that are performed by "processTL" itself. The routines analyze the 3D data at each time point independently. If the aster's filaments are detected, a simple correlation algorithm can extract the MT's dynamic behaviour by identifying corresponding filaments over time. Hence, the tracing of the filaments is the most crucial task. The individual steps that lead to the 3D characterization of a filament are illustrated in **Supplementary Figure 6**.

The automatic processing starts with the mapping of a sphere's surface (**Supplementary Figure 3a,b**) around the centrosome (which is determined by a fluorescence centre of mass calculation). The algorithm determines the intersection points of the MTs with the sphere's surface, thereby providing starting coordinates for the tracing algorithm (**Supplementary Figure 3c**). The choice of the mapping radius is important in several aspects. If the radius is too large, short MTs will be missed. A too small radius, however, will result in the failure of recognizing neighboring MTs as separate filaments (due to the microscope's limited spatial resolution and the CCD camera's limitation in sampling). Typically, a mapping radius of 5 µm constitutes a good starting value.

Each intersection point belongs to a different MT and is thus processed individually. The tracing of the contour is performed bidirectionally by scanning an angular range around the normal vectors of the spherical surface (with a scan line length of typically 20 pixels, corresponding to 2.58 µm in our 3D data sets), starting at the initial coordinate derived by spherical mapping (**Supplementary Figure 3d**). The algorithm computes the direction characterized by the maximum average light intensity. Inward tracing yields the geometry down to the centrosome, outward tracing leads to the MT's plus-end. A relatively large angular range (typically 15°) is taken into account in the first tracing step, since the MT might actually be oriented towards the mapping surface at an angle that differs from 90°.

Subsequently, the algorithm goes a small step (typically 5 pixels, corresponding to 645 nm in our 3D data sets) in the direction of maximum average light intensity (**Supplementary Figure 3e**), unless the MT's plus-end is close to the mapping surface. The next

tracing steps are performed by scanning a smaller angular range (typically 5°), giving consideration to the polymer‘s physical stiffness. Thereby, the risk of obtaining un-physiological 3D geometries (i.e. processing artifacts) is significantly reduced. The inward tracing is iterated until a coordinate set sufficiently close to the centrosome is reached. At this point, the inward tracing is stopped and the centrosome‘s centre is registered as the MT’s minus-end (**Supplementary Figure 3f**).

Additional statistical criteria are introduced for the outward tracing (i.e. the tracing towards the MT plus-end), since the MT‘s plus-end is considerably more difficult to identify than the centrosome’s centre of mass. Our approach for MT plus-end detection requires the analysis of the normal planes at all outward tracing points with respect to the last tracing direction. Nine normal planes (at a spacing of one pixel, i.e. 129 nm in our 3D data sets) are extracted and averaged (**Supplementary Figure 3g**). Next, the standard deviation of the intensity in the averaged plane is calculated. This value is compared to the standard deviation that results if the analyzed plane contains only background fluorescence. Thus, a tracing point past the MT’s plus-end tip has been reached, if the standard deviation drops below the threshold level (“tracing overshoot”, **Supplementary Figure 3h**). Alternatively, the recording volume‘s boundaries might have been reached, triggering tracing abortion. In the case of a tracing overshoot (which is the standard case for a MT that is located inside the recording volume) the algorithm goes back to the last tracing coordinate and performs a pixel-by-pixel tracing. The last coordinate, for which a standard deviation above the threshold is derived, is defined as the MT‘s plus-end (**Supplementary Figure 3i**).

Using this approach, a set of discrete tracing points from the centrosome‘s centre up to the MT‘s plus-end is obtained. Typically, analysis routines for dynamic instability or MT mechanics measurements are applied next. An example of an interphase aster data set (MT contours for one time point of the time-lapse recordings) that has been digitalized by “processTL” is shown in **Supplementary Video 4**.

While we observed a good performance of this algorithm in data sets of sufficiently high quality (characterized by a good signal-to-noise level along the MT filaments), several

robustness issues should be pointed out. The contour detection can be impaired by local inhomogeneities in the recording volumes, e.g. fluorescent protein clusters. MT contact or MT bundling may lead to contour recognition errors. While we systematically avoided the use of empirical parameters, we considered a manual adjustment of the deviation threshold (which serves as the plus-end detection criterion), depending on the quality of the recordings. A data set of low quality (i.e. with a low signal-to-noise ratio) is far more sensitive to this parameter than a high-quality data set. In contrast, the semi-automated tracing approach ("defineMT") proved to be highly reliable and significantly more robust on data with low signal-to-noise ratios. In order to provide consistent data – in particular for the side-by-side comparison of 2D and 3D experiments –, we performed the contour analysis with the "defineMT" routines.

Supplementary References

[1] Murray, A.W. 1991. Cell cycle extracts. *Methods Cell Biol*. 36:581-609.

[2] Parsons, S.F. and E.D. Salmon. 1997. Microtubule assembly in clarified *Xenopus* egg extracts. *Cell Motil Cytoskeleton*. 36:1-11.

[3] Greger, K., Swoger, J. and E.H.K. Stelzer. 2007. Basic building units and properties of a fluorescence single plane illumination microscope. *Review of Scientific Instruments*. 78.

[4] Gildersleeve, R.F., A.R. Cross, K.E. Cullen, A.P. Fagen and R.C. Williams Jr. 1992. Microtubules grow and shorten at intrinsically variable rates. *J Biol Chem*. 267:7995-8006.